

Performance comparison between multichannel polychromatic and conventional joint transform correlators

Chih-Sung Wu

Chulung Chen, MEMBER SPIE

Yuan Ze University

Department of Electrical Engineering

135 Yung Tung Road

Taoyuan 320, Taiwan

E-mail: chulung@saturn.yzu.edu.tw

Abstract. We design a multichannel polychromatic nonzero-order joint transform correlator (NOJTC). The system is implemented using a general JTC scheme by the design of an ideal reference function and additional power-spectrum subtraction strategy for a multichannel correlator. We test the performance for noise and distorted images in the input. In addition, the introduction of various numbers of images in the training set is investigated. The multichannel polychromatic NOJTC shows better detection ability over conventional systems. © 2003 Society of Photo-Optical Instrumentation Engineers. [DOI: 10.1117/1.1571060]

Subject terms: nonzero order joint transform correlator; multichannel correlator; power-spectrum subtraction.

Paper 020339 received Aug. 6, 2002; revised manuscript received Nov. 11, 2002; accepted for publication Nov. 12, 2002.

1 Introduction

With the help of electronic devices, optical correlation for pattern recognition has many advantages, e.g., programmable, real-time, and parallel processing capabilities. Since the introduction of the holographic matched filter by Vander Lugt,¹ techniques, experiments, architectures, and algorithms have been developed to construct efficient optical correlators for pattern recognition application. Today, the most common techniques used for optical pattern recognition are the Vander Lugt's correlator (VLC) based systems that use Fourier domain matched filtering and joint transform correlators (JTCs)² that use spatial-domain filtering. Both of these correlators have the property of shift invariance that can be used for targets tracking in pattern recognition. Some advantages of both systems have been investigated in the literature.³ However, in the Vander Lugt's setup, one has to consider the accurate alignment issue along the optical axis. On the other hand, the JTC system arranges the reference and the target side by side at the input plane, reducing the system alignment requirement. Nevertheless, in a conventional JTC, the joint transform power spectrum (JTSP) has a large zero-order part, which results in lower detection efficiency, particularly when applied to the recognition of multiple objects or targets with background noise.⁴ To improve correlation efficiency, Javidi and Kuo⁵ introduced a binary JTC, with high correlation peak intensity, a high correlation discrimination ratio, and narrow correlation width when compared with conventional JTCs. The fringe-adjusted filter (FAF) proposed by Alam and Karim^{6,7} also provides a solution to improve the efficiency. To eliminate the dc term, some methods have been proposed and demonstrated in the literature.⁸⁻¹⁰ An algorithm called the JTSP subtraction technique¹¹ is applicable for the hybrid-optical JTC system. In this work, a generalized zero-order term removal strategy is proposed.

In the topic of distortion-invariant pattern recognition, Alam, Chen, and Karim¹² adopted the distortion-invariant FAF JTC. However, there is no theoretical guarantee that this algorithm will converge to a solution in every case. Recently, Chen and Fang¹³⁻¹⁵ adopted the technique of Lagrange multipliers to design a reference function that can produce sharp correlation peaks for monochromatic images.

Besides shapes, colors are fundamental characteristics of concern in pattern recognition. In most cases, VLCs and JTCs are implemented to handle monochromatic images. In the real world, most visual signals are actually composed of color information, which motivates the development of color pattern recognition.¹⁶⁻¹⁸ Therefore, the idea of a multichannel JTC has been proposed.^{19,20} To achieve color pattern recognition, Deutsch, Garcia, and Mendlovic²¹ introduced a multichannel single-output JTC by the rearrangement of objects for all color channels at the input plane. Similar to conventional JTCs, this architecture led to an even larger zero-order part formed by six autocorrelation terms that resulted in poor detection efficiency. Subsequently, to solve the strong dc term problem, Wu, Chen, and Fang²² introduced an improved multichannel NOJTC system for color pattern recognition. More recently, to obtain better performance in a multichannel single-output JTC, Alam and Wai²³ designed a color pattern recognition system where a FAF is utilized. Still, the convergence issue of the algorithm must be investigated further.

In this work, a linearly constrained optimization algorithm for performing multichannel color pattern recognition is proposed by the use of an NOJTC, which has many advantages over other monochromatic or conventional systems. The procedure is shown systematically to obtain the desired optimized function. Afterward, the system is studied with distorted images, noisy images, and various train-

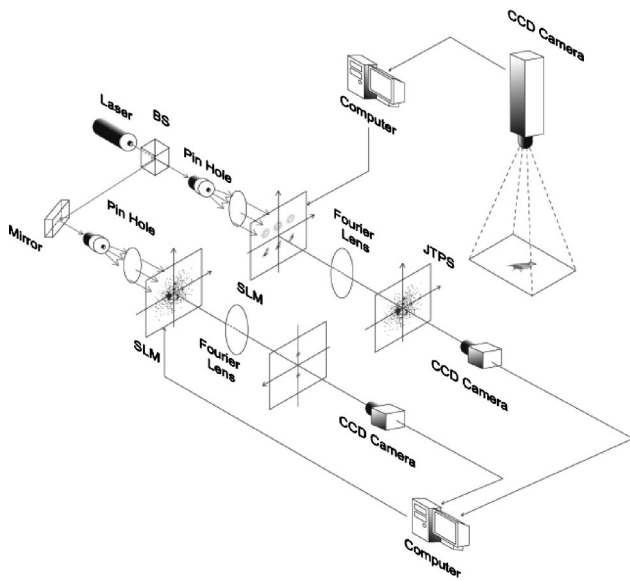


Fig. 1 A multichannel polychromatic NOJTC system.

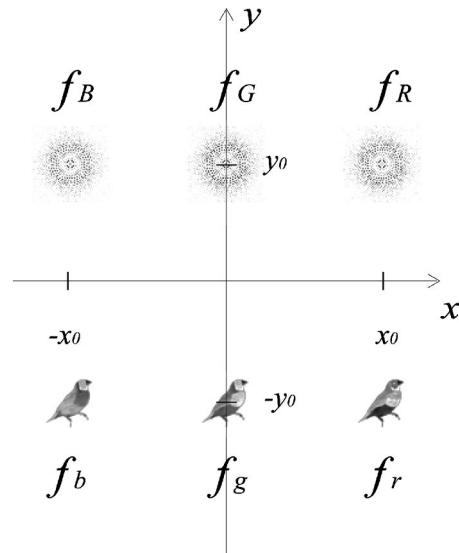


Fig. 2 Arrangement of the red, green, and blue channels at the input plane of a multichannel polychromatic NOJTC.

ing image sets. The proposed correlator has superior discrimination ability.

2 Theoretical Analysis

2.1 Multichannel Polychromatic NOJTC System

The basic architecture of our hybrid-optical NOJTC system is based on Yu and Lu's JTC scheme²⁴ and the multichannel architecture proposed by Deutsch, Garcia, and Mendlovic.

The implementation of our hybrid-optical JTC system is shown in Fig. 1. This optoelectronic hybrid system consists of two spatial light modulators (SLMs) and three CCD cameras. A CCD located at the top right quadrant captures the color target image and forwards it to a computer for RGB color channel separation. The computer transfers grayscale images of RGB color components of both the reference and test images to the first SLM. A laser beam illuminates the electrically addressed SLM comprising the joint input images, which is exactly at the front focal plane of the Fourier lens. Instantaneously, a CCD camera located at the back focal plane of the first Fourier lens can capture the JTPS. A computer for the subsequent JTPS subtraction strategy to remove the zero-order term reads the captured digital information and transfers the processed signal to the second SLM for the inverse Fourier transform. Finally, the CCD camera at the back focal plane of the second Fourier lens can obtain the cross-correlation output with desired peaks only.

2.2 Analysis

The joint input image consists of six grayscale objects: the upper part contains RGB channels from the synthesized reference image, and the lower part involves the corresponding input test scene [see Fig. 2]. The correlation distribution at the output plane, which has been described in detail elsewhere,¹⁹ can be written as

$$O(x', y') = \sum_m \sum_n C_{mn}[x' + (x_m - x_n), y' + (y_m - y_n)], \quad (1)$$

where $n, m \in \{R, G, B, r, g, b\}$ is the position subscript of either the reference image (R, G, B) or the test image (r, g, b) in the input, and C_{mn} represents the correlation between any pair of input objects.

Apparently, the distribution of correlation output depends on the locations of objects at the input plane. Let $(x_R, y_R) = (x_0, y_0)$, $(x_G, y_G) = (0, y_0)$, $(x_B, y_B) = (-x_0, y_0)$, $(x_r, y_r) = (x_0, -y_0)$, $(x_g, y_g) = (0, -y_0)$, and $(x_b, y_b) = (-x_0, -y_0)$. The output plane of the multichannel JTC is shown in Fig. 3. The subscripts in uppercase and lowercase letters represent the reference and target images, respectively. Among these cross-correlation terms are some desired parts in the areas around $(0, 2y_0)$ and $(0, -2y_0)$ shown in Fig. 3, which are expected to yield sharp peaks for targets.

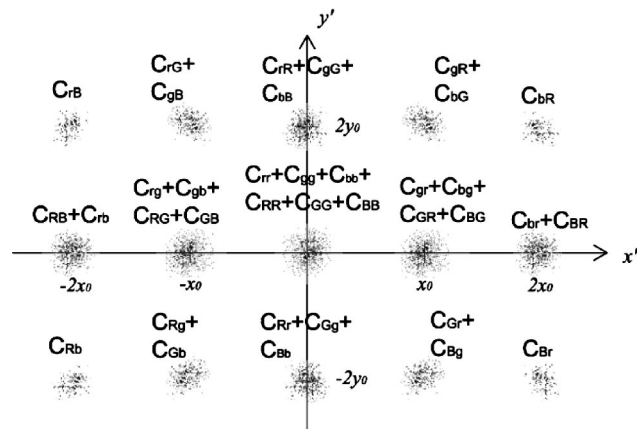


Fig. 3 Locations of the correlation terms at the output plane. Uppercase subscript letters refer to color channels of the reference functions, and lowercase letters represent those of the target.

To solve the problem of a strong zero-order peak appearing at the output plane, which might make the desired correlation signal hard to detect, a JTPS subtraction technique is applied. The idea of this strategy is based on the fact that the JTPS can be stored and calculated individually. The removal procedure is stated as follows:

1. Display the following possible combinations of reference and input images one by one at the input plane and store the corresponding power spectra in the computer. The sets of participating images include $\{f_R, f_G, f_B, f_r, f_g, f_b\}$, $\{f_R, f_G, f_B\}$, $\{f_r, f_g, f_b\}$, $\{f_R, f_g\}$, $\{f_R, f_b\}$, $\{f_G, f_r\}$, $\{f_G, f_b\}$, $\{f_B, f_r\}$, $\{f_B, f_g\}$, $\{f_R\}$, $\{f_G\}$, $\{f_B\}$, $\{f_r\}$, $\{f_g\}$, and $\{f_b\}$.

2. Reshape the desired power spectrum by

$$\begin{aligned}
 I(\alpha, \beta) = & \varepsilon(f_R, f_G, f_B, f_r, f_g, f_b) - \varepsilon(f_R, f_G, f_B) - \varepsilon(f_r, f_g, f_b) \\
 & - \varepsilon(f_R, f_g) - \varepsilon(f_R, f_b) - \varepsilon(f_G, f_r) - \varepsilon(f_G, f_b) \\
 & - \varepsilon(f_B, f_r) - \varepsilon(f_B, f_g) + [\varepsilon(f_R) + \varepsilon(f_G) + \varepsilon(f_B) \\
 & + \varepsilon(f_r) + \varepsilon(f_g) + \varepsilon(f_b)]/2, \quad (2)
 \end{aligned}$$

where, for example, $\varepsilon(f_R, f_G, f_B)$ is the power spectrum due to the presence of f_R , f_G , and f_B together. In fact, Eq. (2) can be shown as

$$\begin{aligned}
 I(\alpha, \beta) = & F_r(\alpha, \beta) F_R^*(\alpha, \beta) \exp[i\alpha(x_R - x_r) + i\beta(y_R - y_r)] \\
 & + F_g(\alpha, \beta) F_G^*(\alpha, \beta) \exp[i\alpha(x_G - x_g) \\
 & + i\beta(y_G - y_g)] + F_b(\alpha, \beta) F_B^*(\alpha, \beta) \\
 & \times \exp[i\alpha(x_B - x_b) + i\beta(y_B - y_b)] \\
 & + F_r(\alpha, \beta) F_r^*(\alpha, \beta) \exp[i\alpha(x_r - x_R) + i\beta(y_r - y_R)] \\
 & + F_G(\alpha, \beta) F_g^*(\alpha, \beta) \exp[i\alpha(x_g - x_G) \\
 & + i\beta(y_g - y_G)] + F_B(\alpha, \beta) F_b^*(\alpha, \beta) \\
 & \times \exp[i\alpha(x_b - x_B) + i\beta(y_b - y_B)], \quad (3)
 \end{aligned}$$

where F_n denotes the Fourier transform of f_n .

3. Send the previous power spectrum to the SLM and obtain the correlation output.

Finally, the field distribution without a zero-order term at the output correlation plane will be

$$\begin{aligned}
 O(x', y') = & C_{Rr}[x' + (x_R - x_r), y' + (y_R - y_r)] \\
 & + C_{Gg}[x' + (x_G - x_g), y' + (y_G - y_g)] \\
 & + C_{Bb}[x' + (x_B - x_b), y' + (y_B - y_b)] \\
 & + C_{rr}[x' + (x_r - x_R), y' + (y_r - y_R)] \\
 & + C_{gG}[x' + (x_g - x_G), y' + (y_g - y_G)] \\
 & + C_{bB}[x' + (x_b - x_B), y' + (y_b - y_B)]. \quad (4)
 \end{aligned}$$

In addition, if one can predesign reference functions for each channel, the intensity distribution captured by the CCD camera at the output plane could be δ -like functions. In pattern recognition, it is quite important to detect the target with different geometric distortion. A particular frequency domain filter¹⁰ is designed to deal with expected distortions and to reduce correlation sidelobes for monochromatic images. This concept has been accomplished by

minimizing the average correlation energy of all training images while keeping the desired correlation peaks at a specified height. Similar techniques can be found in the literature.¹³⁻¹⁵

For the sake of simplicity, a compact style notation is utilized in the following paragraph. Let f_{ki} and h_k be the i 'th training image and the reference image with d pixels at the input plane; and F_{ki} and H_k be the corresponding Fourier transforms, respectively. From the preceding assumption, k actually refers to any of the RGB channels in the color images. The presumption is that there are N centered training images spanning the investigated distortion-invariant feature set. Since the basic correlation property states that $f_{ki} \otimes h_k$ and $F_{ki}^* H_k$ form a Fourier transform pair, the correlation peak for each training image can be written in matrix-vector notation:

$$\hat{F}_k^T \hat{H}_k^* = [c_{k1}(0,0) \ c_{k2}(0,0) \ \dots \ c_{kN}(0,0)]^T = \hat{P}_k, \quad (5)$$

where \hat{F}_k is a matrix with N column vectors in which each column vector represents the discrete version of F_{ki} ; \hat{H}_k denotes the discrete version of H_k ; and \hat{P}_k is the correlation peak requirement of size N with $c_{ki}(0,0)$ as entries, which can be specified as the same to yield equal correlation peaks in response to all training images.

By Parseval's theorem, the average cross-correlation energy function can be described as follows:

$$E_k = \hat{H}_k^T \hat{A}_k \hat{H}_k^*, \quad (6)$$

where \hat{A}_k is a real-valued diagonal matrix whose diagonal entry is $|F_{ki}(\alpha, \beta)|^2/N$. Using the method of Lagrange multipliers, the energy function given in Eq. (6) while satisfying the constraints in Eq. (5) for each channel can be solved. The solution turns out to be

$$\hat{H}_k = \hat{A}_k^{-1} \hat{F}_k (\hat{F}_k^+ \hat{A}_k^{-1} \hat{F}_k)^{-1} \hat{P}_k^*, \quad k = R, G, B, \quad (7)$$

where the superscript $+$ denotes the conjugate transpose.

The inversion of \hat{A}_k is simple, since it is a diagonal matrix. Moreover, $\hat{F}_k^+ \hat{A}_k^{-1} \hat{F}_k$ is of size $N \times N$, and its inversion is not complicated. Therefore, the computation of \hat{H}_k is not difficult. The algorithm converges. No iteration is needed.

The optimum solution in Eq. (7) is a vector representation in the frequency domain. By rearranging the column vector \hat{H}_k as a square matrix H_k , the final optimum reference function in the spatial domain is constructed by

$$h_k(x, y) = \mathcal{J}^{-1}\{\hat{H}_k(\alpha, \beta)\}, \quad k = R, G, B, \quad (8)$$

where \mathcal{J}^{-1} denotes the inverse Fourier transform.

2.3 Performance Criteria

For further investigation on performance, some evaluation criteria are used. The sharpness of the correlation peak can be measured with the peak-to-correlation energy (PCE) ratio at the desired area, which is defined as



Fig. 4 R(top), G(middle), B(bottom) components of four-color images from the original training set, shown in grayscale.

$$\text{PCE} = \frac{\text{desired peak intensity}}{\text{correlation plane energy}}. \quad (9)$$

Thus, it can be seen that the sharper the correlation profile, the higher the accuracy of target detection. Another important aspect in pattern recognition is the peak-to-sidelobe ratio (PSR) at the desired area, as given by

$$\text{PSR} = \frac{\text{desired peak intensity}}{\text{maximum sidelobe}}. \quad (10)$$

In this equation, the sidelobe (or the secondary peak) is defined to be the highest intensity point in the correlation plane at points at least two pixels away from the peak location. The PSR diagram further denotes the recognition possibility of the correlator. Practically, in our study, PSR values less than 1.5 are considered unrecognizable.

On the topic of an antinoise performance evaluation, the signal strength can be specified by the signal-to-noise ratio (SNR), which is defined as follow:

$$\text{SNR} = \frac{\text{total signal power}}{\text{total noise power}} = \frac{\sum_i S_i^2}{d \cdot \sigma^2}, \quad (11)$$

where S_i is the amplitude of the signal at pixel i , σ^2 is the variance of each pixel, and d is the pixel number.

3 Numerical Results

For comparison, a multichannel polychromatic JTC and a multichannel polychromatic NOJTC are studied in the initial test. In the pattern recognition process, images can be affected by various kinds of degradation. Hence, input images with various degrees of noise are investigated next. The noise performance of a multichannel polychromatic NOJTC is compared with those of a FAF NOJTC and a single-channel monochromatic JTC. Furthermore, the capability of distortion invariance is studied in the third part of the simulation. Finally, the values of PCE and PSR with respect to various numbers of training images to design the reference function are illustrated.

In the beginning experiment, there are 24 color images in the original training set, which is assumed to be descrip-

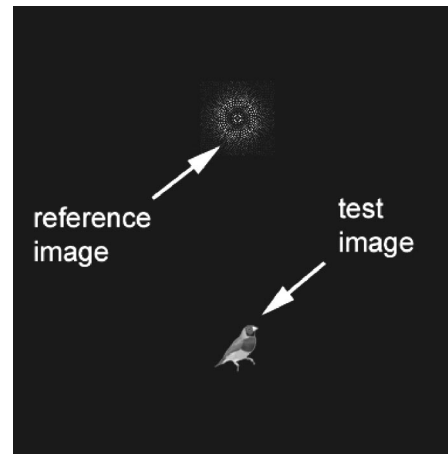


Fig. 5 The input scene of a monochromatic NOJTC. The input scene is 384×384 pixels.

tive of possible distorted target images (the capacity is changed in a later investigation). Therefore, for each channel, there are 24 training images to synthesize the associated reference function. Some examples are shown in Fig. 4. To avoid overlapping the correlation distribution at the output plane, each target image or reference image in the input scene consists of 64×64 pixels, while the vertical and horizontal separations are chosen to be 128 and 64 pixels, respectively.

In this optoelectronic system, the optical Fourier transform is real time, while the duration of the reference image synthesis and the electronic transfer of JTPS achieved by computer are machine dependent. To improve the speed of the system, the transfer speed of JTPS can be improved by designing a special interface.

3.1 Result for a Noise-Free Input Image

The target object in this work is chosen to be a color image from a bird, Lady Gould. The synthesized reference image composed of 24 rotating images from the target is actually generated using Eq. (7). The overall size of the input scene in each correlator is 384×384 pixels. The input image is partitioned into two parts: the reference image at the top, and the test image at the bottom, as seen in Fig. 5. The correlation output of this system after applying the JTPS

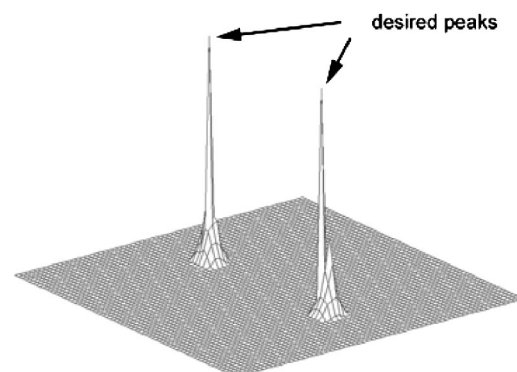


Fig. 6 The 3-D correlation intensity profile of a monochromatic NOJTC.

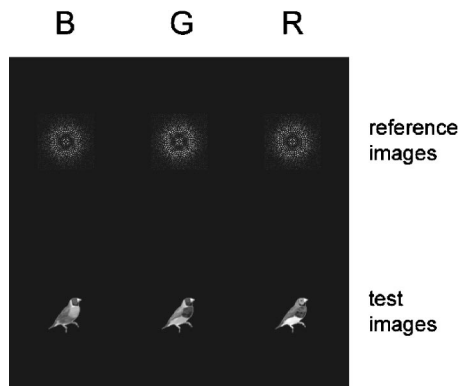


Fig. 7 The joint input plane for multichannel polychromatic JTCs. The dimension of the input scene is 384×384 pixels.

subtraction procedure should contain two sharp peaks located, respectively, at areas around $(0, -2y_0)$ and $(0, 2y_0)$ (see Fig. 6).

The greatest difference between the architectures of the single-channel monochromatic JTC and the multichannel polychromatic JTC is the joint input image. They are different in the number of input plane objects. The joint input image of a multichannel polychromatic JTC is composed of three channels, in the order of red, green, and blue, arranged from right to left. The upper part of each channel includes the reference image, while the lower part contains the corresponding input scene (see Fig. 7). From the preceding analysis, the regions of interest at the output plane are the areas around $(0, -2y_0)$ and $(0, 2y_0)$, as shown in Fig. 8. All peaks in the graph of correlation intensity are normalized according to the highest peak for the reason of observation. However, no appreciable peaks could be found in these areas. In contrast to the flat desired areas, the zero-order parts are quite strong. According to our numerical analysis from the output spectra of the multichannel color JTC, the zero-order peak can be about 8816 times higher than the desired ones. The input scene of the multichannel polychromatic NOJTC is actually the same as in the previous one. Still, the regions of interest are the areas around $(0, -2y_0)$ and $(0, 2y_0)$, as shown in Fig. 9. With the help of a JTPS subtraction technique, peaks other than the desired ones are noticeably eliminated.

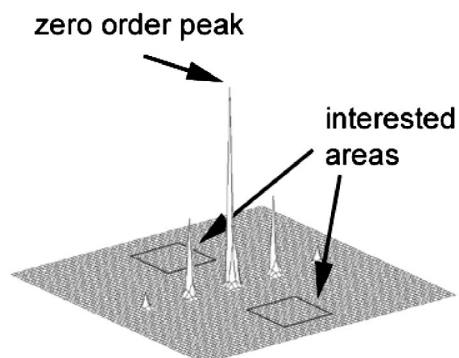


Fig. 8 The 3-D correlation intensity profile of a multichannel polychromatic JTC.

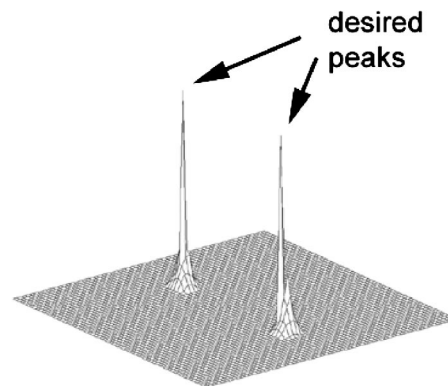


Fig. 9 The 3-D correlation intensity profile of a multichannel polychromatic NOJTC. All unwanted terms have been removed.

It takes 20 sec to synthesize all three reference functions of the multichannel system from 24 color images. The algorithm converged. In the FAF NOJTC, the correlation performance is excellent when the number of training images is small. However, the relaxation constant is selected by trial and error. When the constant is large (e.g., 1) and the number of training images becomes large (e.g., 24), the system might diverge. As we selected 0.01 as the relaxation constant, it took 40 iteration (6.6 sec) to reach a local minimum. As more iterations went on, the system diverged, then converged, and so on.

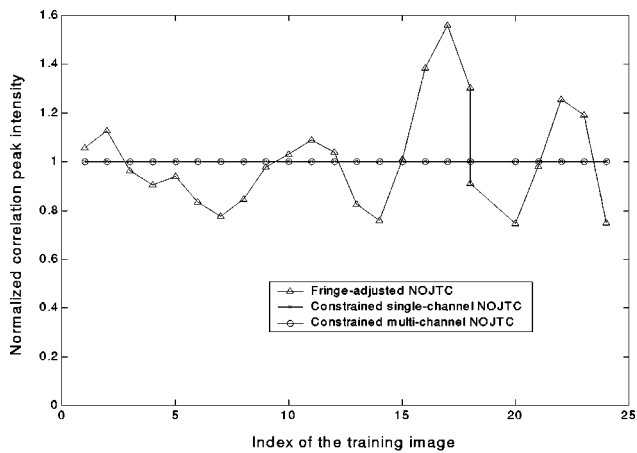
3.2 Results for Distorted Multiple Images and Noisy Images

The recognition of distorted multiple images and noisy images is of interest in many applications. The distortion-invariant characteristics of the three correlators (a FAF NOJTC, a single-channel monochromatic NOJTC, and a multichannel polychromatic NOJTC) are studied here.

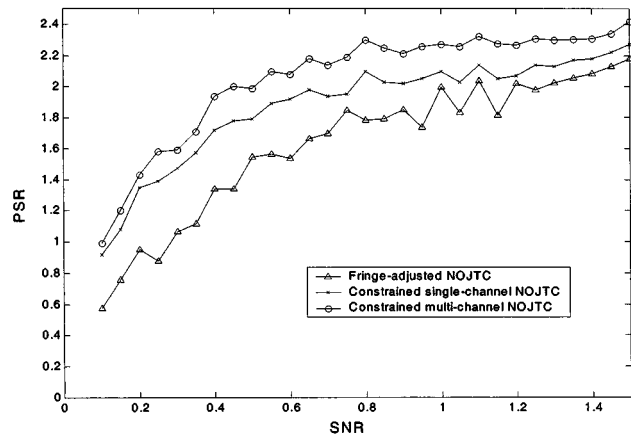
Figure 10 depicts the common input image composed of three birds. One nontarget bird is located at the bottom left quadrant of the input image with two rotated targets aside. After optoelectronic processing, all three systems yield acceptable result to detect targets and discriminate against nontargets. Exactly two sharp peaks for the two systems exist at either of the desired areas in the output plane. The correlation outputs show almost no difference by inspection and therefore are not shown here. According to the numerical analysis, the PCE values are 0.0056, 0.0207, and 0.0235 for the FAF, the single-channel, and the multichannel NOJTCs, respectively. The FAF method yields the lowest, since it assumes that the reference function is a linear combination of the training images. This is somewhat conve-



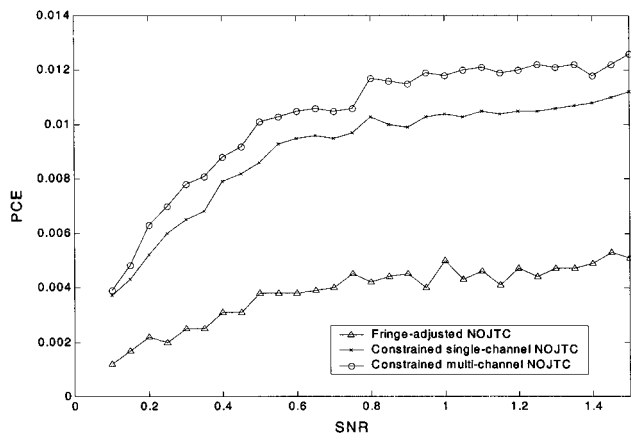
Fig. 10 R (left), G (middle), B (right) components of a test image, which is composed of three objects for distorted multiple investigations. A nontarget bird is located at the bottom left corner with two rotated targets aside.



(a)



(b)



(c)

Fig. 11 (a) Normalized correlation peak intensity as a function of the index of the 24 training images for different correlators. (b) PSR and (c) PCE as functions of input SNR for different correlators.

nient in the design determining only N weights. However, it limits the degree of freedom of possible solutions. We also believe that the correlation energy cannot be effectively suppressed.

The normalized correlation peak intensity with respect to the 24 training images is shown in Fig. 11(a). Peak intensities are the same for the single-channel JTC and the



Fig. 12 R (left), G (middle), B (right) components of an input test scene with background. The target bird is located in the bottom left quadrant.

multichannel NOJTC. The FAF algorithm fails to maintain the uniformity of the correlation peak responses.

Moreover, to test the noise performance, some random noise is added to the input image. Comparison between the three correlators is analyzed. The amount of input noise is determined by the SNR value. As the SNR increases, the amount of noise decreases. PSR and PCE plots are illustrated in Figs. 11(b) and 11(c), respectively. Both plots show the result for average values more than 100 times of random noise sampling. The more sampling times, the smoother the curve obtained. By recalling the definition of PSR in Eq. (10), the PSR value should be larger than, say, 1.5 for efficient recognition. It comes out that the part with SNR smaller than 0.5 is not interested in the FAF method, since the target cannot be recognized. One can find that the multichannel color NOJTC is somewhat better than the monochromatic NOJTC. Due to the reason described, the part with SNR less than 0.3 in Fig. 11(c) is not of our concern. Still, the multichannel polychromatic NOJTC is better than the monochromatic NOJTC in the interval of interest.

In addition, another input image with jungle background and an additional bird (nontarget) at the right-hand side of the target is tested, as illustrated in Fig. 12. The forest background is added independently at the bottom layer of the test image. It can be seen that the nontarget bird and the target bird belong to the same species with nearly identical color spots. The corresponding 3-D correlation profiles of the two correlators are plotted respectively in Figs. 13(a) and 13(b). The sidelobes are larger due to the increasing background signal energy. However, all desired correlation peaks appear in recognizable shapes. According to the numerical analysis, the multichannel polychromatic NOJTC exceeds the monochromatic NOJTC in PCE value by 18% and PSR value by 37% in this case. The FAF performance is the least.

3.3 Effect for Increasing the Number of Training Set Images

The more training images used in the procedure to produce the reference image, the greater the recognition capacity of the system will be. However, expanding the training images results in the magnification of sidelobes. To clarify the behavior of the monochromatic and multichannel NOJTCs, the PCE and PSR diagrams are plotted. Figure 14 illustrates the PCE as a function of the number of training images to synthesize the reference function for the two cases. On the other hand, the plot of PSR is shown in Fig. 15. The results are obtained by generating the reference images from 10 to 360 training images at an increment of 10 images and testing it on the same image investigated in Sec. 3.1. As the

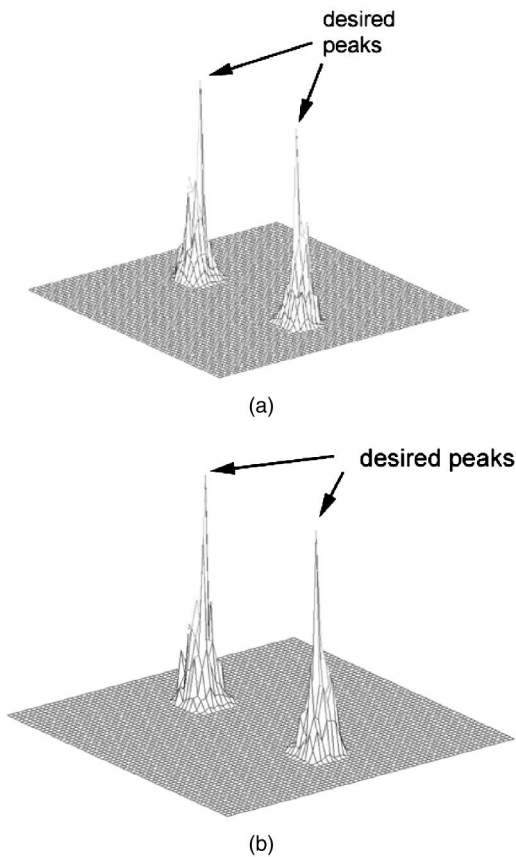


Fig. 13 The 3-D correlation intensity profile of Fig. 12 with (a) a multichannel polychromatic NOJTC and (b) a single-channel monochromatic NOJTC.

number of training images increases, the number of constraint equations increases. The ratios decrease due to the increase of the correlation output energy.

Both the PCE and PSR ratios are about 25% better than the monochromatic NOJTC for the target being tested. These figures show that the multichannel single output NOJTC yields better discrimination performance on the

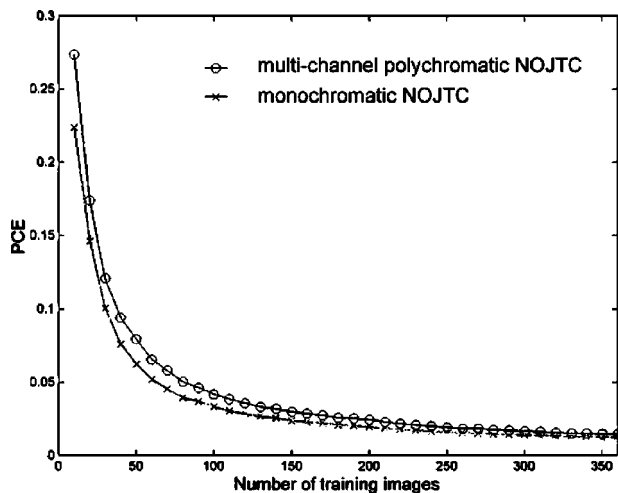


Fig. 14 PCE as a function of the number of training images for two different correlators.

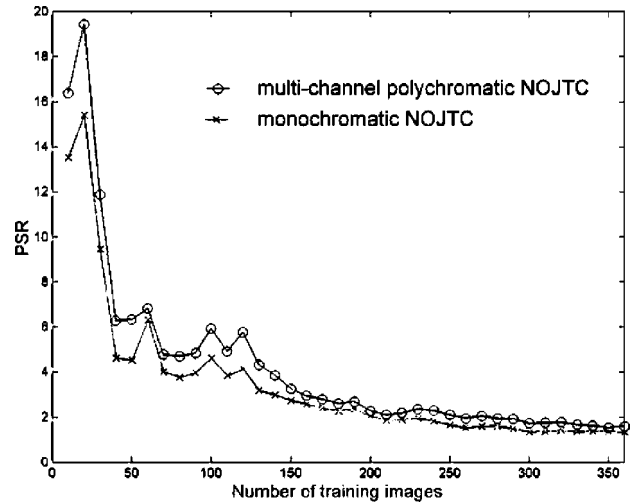


Fig. 15 PSR as a function of the number of training images for two different correlators.

tested training images than the monochromatic NOJTC. However, more studies have to be investigated to confirm this point.

3.4 Rearrangement of Input Scene

Without the zero-order part at the output plane, color pattern recognition with an NOJTC could be easier and the system could be smaller when compared with the conventional multichannel JTC setup, since the arrangement of input objects could be closer. This is illustrated as follows. The rearranged joint input scene is shown in Fig. 16(a) while the output is shown in Fig. 16(b). The sizes of the two figures are both 192×192 pixels. As a result, after

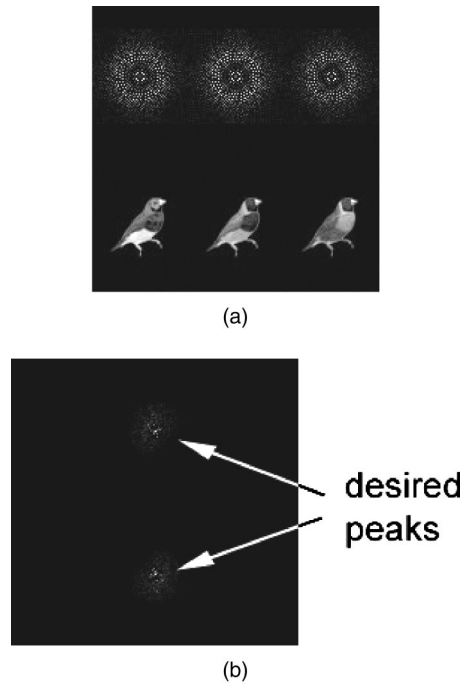


Fig. 16 (a) A rearranged joint input scene, and (b) the output plane. The dimension of the input scene is 192×192 pixels.

adopting the JTPS subtraction technique, both the input and output planes can be smaller as compared to Figs. 7 and 8.

4 Conclusion

In this study, a multichannel color pattern recognition method using an NOJTC is presented. Theoretically, the system improves the performance of a JTC in terms of better pixel utilization (compared with conventional multichannel JTCs), distortion invariance, higher detection efficiency, and better noise tolerance ability. Furthermore, to evaluate the performance of recognition capability (the normalized correlation peak intensity), PCE and PSR have been used as metrics in our study.

Like most optical correlators, our system offers the capability of real-time processing. We have used the SLMs. One advantage of this equipment is the programming ability. By connecting to a computer, we are able to change the information displayed at the SLMs in an efficient way. In other words, motion target recognition is applicable in our system.

The proposed method has been demonstrated by the use of RGB color channels, but it can be modified to adapt more channels. Since the increase in channels yields better performance in our study, the application of additional thermal or infrared channels may be a good subject for further investigation. In addition, by suppressing the zero-order part at the output plane, color pattern recognition with an NOJTC could be easier and the system could be smaller when compared with the conventional multichannel JTC, since the arrangement of input objects could be closer. Nevertheless, the implementation of multichannel input images still involves the requirement of a larger SLM and costs more than the single-channel JTC. The improvement on PCE and PSR ratios for the multichannel color NOJTC system, however, differs from case to case. So far, the value varies from 5 to 40% in our considerable simulations. We believe that the result is general, but more analytical evidences in mathematics are necessary to confirm this point.

Acknowledgments

This research has been supported by the National Science Council, Republic of China, under grants NSC 90-2215-E-155-006 and NSC 91-2215-E-155-001.

References

1. A. Vander Lugt, "Signal detection by complex spatial filtering," *IEEE Trans. Inf. Theory* **10**, 139–146 (1964).
2. C. S. Weaver and J. W. Goodman, "A technique for optically convolving two functions," *Appl. Opt.* **5**, 1248–1249 (1966).
3. X. J. Lu, F. T. S. Yu, and D. A. Gregory, "Comparison of VanderLugt and joint transform correlator," *Appl. Phys. B: Lasers Opt.* **51**, 153–164 (1990).
4. F. T. S. Yu, Q. W. Song, Y. S. Cheng, and D. A. Gregory, "Comparison of detection efficiencies for Vander Lugt and joint transform correlators," *Appl. Opt.* **29**, 225–232 (1990).
5. B. Javidi and C. J. Kuo, "Joint transform image correlation using a binary spatial light modulator at the Fourier plane," *Appl. Opt.* **27**(14), 663–665 (1988).
6. M. S. Alam and M. A. Karim, "Fringe-adjusted joint transform correlation," *Appl. Opt.* **32**(23), 4344–4350 (1993).
7. M. S. Alam, "Performance of joint transform correlation under vary-

- ing illumination and noise," *Opt. Laser Technol.* **27**, 361–368 (1995).
8. F. Cheng, P. Andres, and F. T. S. Yu, "Removal of intra-class associations in joint power transform spectrum," *Opt. Commun.* **99**, 7–12 (1993).
9. G. Lu, Z. Zhang, S. Wu, and F. T. S. Yu, "Implementation of a nonzero order joint transform correlator by use of phase shifting techniques," *Appl. Opt.* **36**(2), 470–483 (1997).
10. S. Jutamulia and D. A. Gregory, "Soft blocking of the dc term in Fourier optical systems," *Opt. Eng.* **37**(1), 49–51 (1998).
11. C. Li, S. Yin, and F. T. S. Yu, "Nonzero-order joint transform correlator," *Opt. Eng.* **37**(1), 58–65 (1998).
12. M. S. Alam, X. Chen, and M. A. Karim, "Distortion-invariant fringe-adjusted joint transform correlator," *Appl. Opt.* **36**, 7422–7427 (1997).
13. C. Chen and J. S. Fang, "Cross correlation optimization for joint transform correlators," *Opt. Commun.* **178**, 315–322 (2000).
14. C. Chen and J. Fang, "Minimum-variance nonzero order joint transform correlators," *Opt. Commun.* **178**, 315–322 (2000).
15. C. Chen and J. Fang, "Nonzero order joint transform correlator with an optimized real-valued reference function," *J. Mod. Opt.* **48**(8), 1329–1338 (2001).
16. C. Warde, H. J. Caulfield, F. T. S. Yu, and J. E. Ludman, "Real-time joint spectral-spatial matched filtering," *Opt. Commun.* **49**, 241–244 (1984).
17. J. E. Ludman, B. Javidi, F. T. S. Yu, H. J. Caulfield, C. Warde, and U. Efron, "Real-time colored-pattern recognition," *Proc. SPIE* **465**, 143–149 (1984).
18. F. T. S. Yu, Z. Yang, and K. Pan, "Color target identification using a color LCTV based joint-transform correlator," *Appl. Opt.* **33**, 2170–2172 (1994).
19. J. H. Feng, G. F. Chin, M. X. Wu, S. H. Yan, and Y. B. Yan, "Multi-object recognition in a multi-channel joint-transform correlator," *Opt. Lett.* **20**, 82–84 (1995).
20. G. Keryer and J. L. B. Tognaye, "A multi-channel joint transform correlator," *Opt. Commun.* **118**, 102–113 (1995).
21. M. Deutsch, J. Garcia, and D. Mendlovic, "Multi-channel single-output color pattern recognition by use of a joint-transform correlator," *Appl. Opt.* **35**, 6976–6982 (1996).
22. C. Wu, C. Chen, and J. Fang, "Constrained optimization for color pattern recognition with a nonzero order joint transform correlator," *Microwave Opt. Technol. Lett.* **33**, 385–388 (2002).
23. M. S. Alam and C. N. Wai, "Color pattern recognition using fringe-adjusted joint transform correlator," *Opt. Eng.* **40**(11), 2407–2413 (2001).
24. F. T. S. Yu and X. J. Lu, "A real-time programmable joint-transform correlator," *Opt. Commun.* **52**, 10–16 (1984).



Chih-Sung Wu received his BS degree in electrophysics in 1997 from National Chiao Tung University, Taiwan, and his MS degree in electrical engineering in 2002 from Yuan Ze University, Taiwan. He worked in the area of optical color pattern recognition with his adviser, Dr. Chulung Chen. He has published international journal papers in the field of hybrid digital/optical color pattern recognition. Currently, he is a software engineer developing embedded systems.



Chulung Chen received his PhD degree in electrical engineering from Pennsylvania State University in 1997. After that, he served as an assistant professor in the Electrical Engineering Department at Yuan Ze University, Taiwan. Currently, he is an associate professor. His photo and research work appeared in an American local newspaper in 1996, in which he was reported as one of two scientists to study heart disease by electro-optics technique. He has published more than 20 international journal papers in the field of hybrid digital/optical image processing, pattern recognition, and biomedical optics. He is a member of SPIE and OSA.